Sādhanā (2021)46:111
https://doi.org/10.1007/s12046-021-01635-y

Identification of practical spindle-tool interface parameters using an optimization based statistical approach

JAKEER HUSSAIN SHAIK[1,*], J SRINIVAS[2], T SRINIVAS RAO[3], K RAMA KOTAIAH[4] and B RAGHU KUMAR[5]

[1]Department of Mechanical Engineering, Malla Reddy Engineering College, Secunderabad, Telangana, India
[2]Department of Mechanical Engineering, National Institute of Technology Rourkela, Rourkela, India
[3]Department of Mechanical Engineering, Vasireddy and Venkatadri Institute of Technology, Guntur, India
[4]Department of Mechanical Engineering, KKR & KSR Institute of Technology and Sciences, Guntur, India
[5]Department of Mechanical Engineering, P.V.P Institute of Technology, Vijayawada, India
e-mail: jakeershaik786@yahoo.co.in; srin07@yahoo.co.in; sr.tanneeru@gmail.com; krk.kits@gmail.com; braghu5051@gmail.com

MS received 6 October 2018; revised 15 February 2021; accepted 19 April 2021

Abstract. The dynamic performance of a high-speed machine tool spindle primarily depends on the rigidity between the spindle-holder couplings. The machining stability of such system is determined by the rigidity at the tapered portion of the coupled joints. This paper presents a methodology to evaluate tool-tip frequency response function (FRF) by considering the tool holder-spindle interface stiffness using finite element analysis. Furthermore, a comparative analysis is carried out on the spindle-tool system with constant contact spring stiffness and the variable structural damping factors. This approach is applied to identify the correct set of interface parameters of a practical spindle-tool unit using the experimental test data. An effective optimization strategy is used to update the finite element model with the various statistical sampling parameters to obtain the rigidity. Further, the optimal data set is identified by using single point simulated annealing (SA) and metaheuristic genetic algorithms (GA) schemes. The proposed methodology can help to standardize the tests with various spindle-holder interfaces by modeling the machine tool spindle.

Keywords. Joint dynamics; spring stiffness; structural damping factors; modal testing; interface parameters; non-conventional optimization.

1. Introduction

The spindle-tool holder coupling forms the most flexible parts in the machine tool structure, which are often not considered during modeling. The primary cause of the chatter vibrations in machining is due to these elastic couplings. In the response signal, when the lower spindle modes come in close proximity with chatter frequency, it results in machining instability [1]. Therefore, an accurate dynamic model of the spindle-tool system is necessary by considering spindle-holder interface elasticity, bearing nonlinearities, initial preload, etc. [2]. In milling point of view, the spindle-tool system generally comprises of spindle, tool holder and tool, such that each element is joined to the other through certain tapered interfacial regions. The variable contact stresses acting at such interfaces results in a distributed elastic force at the junction surface.

For understanding of such interface elasticity effects, analytical and numerical models of spindle-tool systems are very useful. Finite element modeling is the most frequency used approach. Namazi *et al* [3] obtained the interface stiffness data by minimizing the error between the numerical and the experimental frequency responses. An approach to assist the conceptual design of machine tool interfaces for high-speed machining processes was presented by Bossmanns and Tu [4]. The methodologies to evaluate contact stiffness based on the experimental and analytical finite element modeling were presented [5, 6]. The high-speed spindle with thermodynamic characteristics with several spindle–holder arrangements and the corresponding temperatures were evaluated at the interfaces [7, 8]. Various updated numerical models of the spindle tool design systems to predict the dynamic characteristics of the coupling interfaces were proposed [9–11]. The modal characteristics of the angular contact ball bearing spindle tool system with the numerical models as well as with the experiments were investigated

*For correspondence
Published online: 02 June 2021

[12–14]. The overall joint dynamics at the interfaces of spindle-holder coupled structure using the rigid coupling were evaluated by the inverse receptance coupling approach [15, 16]. The centrifugal and gyroscopic effects on the dynamic performance of the rotating high-speed spindles with effects like drawbar were studied [17–20]. Different numerical and empirical approaches to estimate the static stiffness and damping at different interfaces of the spindle and tool holder connections were introduced [21, 22]. The contact stiffness estimation at different locations of the spindle and holder by combining the fractal theory and the classical elastic theory was presented [23]. The joint interfaces were modeled as the flexible elements and the joint dynamic properties are identified by the receptance coupling algorithms [24, 25]. The design procedure of spindle-holder-tool assembly was proposed by modifying the frequency response functions at the tooltip [26]. Recently, Liu *et al* [27] proposed a multi scale contact mechanics model along with fractal theory for predicting analytical contact stiffness between the spindle and tool holder. The micro morphology of rough surfaces was predicted via the fractal theory and concluded that the contact stiffness increases with cutting force. Chang *et al* [28] presented a theoretical model of calculating joint interfacial contact stiffness using fractal theory and transfer matrix method for spindle analysis.

Identification of optimum process parameters in different machining processes has been widely studied. Several optimization schemes were implemented to obtain the optimal cutting conditions during the high-speed machining [29–36]. The model updating via the optimization is one of the recent approaches for achieving the optimum parameters. The frequency response obtained from the spindle-tool model is compared with the experimentally measured response signal. The corresponding deviations are minimized by adjusting the interface stiffness parameters. Present work considers simultaneously the two regional interface effects in spindle-holder-tool of mill-spindle system and identifies the practical interface stiffness parameters. The tool-tip response signal is characterized in frequency domain with some important statistical parameters. By considering the initial values of interface stiffness coefficients, the tool-tip frequency response functions are obtained numerically using finite element modeling. The deviation of frequency response is minimized using two non-conventional optimization schemes namely genetic algorithms and simulated annealing technique. Sensivity study is also performed. The rest of the paper is organized as follows: Section 2 explains the mathematical modeling of an integral system. Section 3 presents optimization approaches considered in the work and section 4 gives the results and discussion part. Conclusions are given in section 5.

2. Modeling of the spindle-tool unit

A schematic diagram of the proposed spindle-holder-tool system supported on two rolling element bearings is shown in figure 1. Due to the rotational symmetry of the configuration, the spindle-tool system is modeled with two noded beam elements.

2.1 *Finite element model of spindle-tool system*

By using the Timoshenko beam formulation having three translational (axial and two bending motions u, v, w) and two rotational degrees of freedom (corresponding slopes θ_y, θ_z) under shear deformation effect, the resultant kinetic and potential energies of the system are given by

$$T = \int_0^L \frac{1}{2} J\rho\Omega^2 dx + \int_0^L \frac{1}{2}\rho A(\dot{u}^2 + \dot{v}^2 + \dot{w}^2)dx + \int_0^L \frac{1}{2} I\rho\left(\dot{\theta}_y^2 + \dot{\theta}_z^2\right)dx + \int_0^L \frac{1}{2} J\rho\Omega\left(\dot{\theta}_y\theta_z + \theta_y\dot{\theta}_z\right)dx \tag{1}$$

$$V = \int_0^L \frac{1}{2} EA\left(\frac{\partial u}{\partial x}\right)^2 dx + \int_0^L \frac{1}{2} EI\left[\left(\frac{\partial \theta_y}{\partial x}\right)^2 + \left(\frac{\partial \theta_z}{\partial x}\right)^2\right]dx + \int_0^L \frac{1}{2} k_s AG\left[\left(\theta_y + \frac{\partial w}{\partial x}\right)^2 + \left(\theta_z - \frac{\partial v}{\partial x}\right)^2\right]dx + \int_0^L \frac{1}{2} EA\left[\left(\frac{1}{2}\left(\frac{\partial v}{\partial x}\right)^2\right)^2 + \left(\frac{1}{2}\left(\frac{\partial w}{\partial x}\right)^2\right)^2\right]dx \tag{2}$$

Where $J = \frac{1}{2}\pi R^4$ is the polar moment of inertia and $I = \frac{1}{4}\pi R^4$ is the moment of inertia. Here, A is the cross-sectional area, Ω is the rotational speed, R is the radius of the beam, ρ is the density of the beam respectively, while k_s is a shear correction factor. The work done by the external forces is expressed as:

$$W = \int_0^L \left(q_x u + q_y v + q_z w + m_y\theta_y + m_z\theta_z\right)dx + \int_0^L \frac{1}{2}\Omega^2 v^2\rho A dx + \int_0^L \frac{1}{2}\Omega^2 w^2\rho A dx \tag{3}$$

Here, (m_x, m_y, m_z) and (q_x, q_y, q_z) are respectively the distributed moments and shear per unit length in x, y, and z

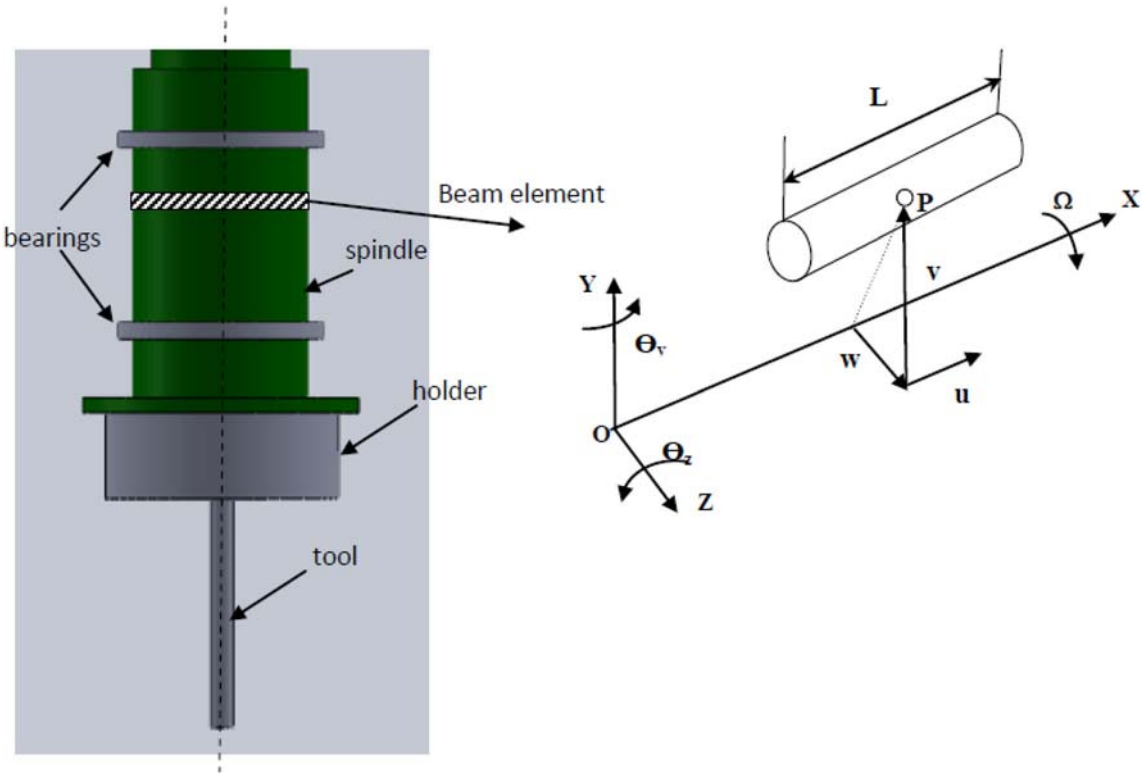

Figure 1. Spindle-tool unit and beam element nomenclature.

directions. The finite element formulation can be given by writing the translational and rotational displacements as:

$$u = [N_a]\{X_e\}$$
$$[\text{v w }]^T = [N_t]\{X_e\}$$
$$[\theta_\text{x}\ \theta_\text{y}]^T = [N_\theta]\{X_e\} \tag{4}$$

where $[N]$ are the shape function matrix and $\{X_e\}$ is the nodal displacement vector. The detailed expressions are given below:

$$[N_a] = [N_{t1}\ \ 0\ \ 0\ \ 0\ \ 0\ \ N_{t2}\ \ 0\ \ 0\ \ 0\ \ 0] \tag{5}$$

$$[N_t] = \begin{bmatrix} 0 & N_{t3} & 0 & 0 & N_{t4} & 0 & N_{t5} & 0 & 0 & N_{t6} \\ 0 & 0 & N_{t3} & -N_{t4} & 0 & 0 & 0 & N_{t5} & -N_{t6} & 0 \end{bmatrix} \tag{6}$$

$$[N_\theta] = \begin{bmatrix} 0 & 0 & -N_{\theta1} & N_{\theta2} & 0 & 0 & 0 & -N_{\theta3} & N_{\theta4} & 0 \\ 0 & N_{\theta1} & 0 & 0 & N_{\theta2} & 0 & N_{\theta3} & 0 & 0 & N_{\theta4} \end{bmatrix} \tag{7}$$

$$\{X_e\} = [\,u_i \quad v_i \quad w_i \quad \theta_{yi} \quad \theta_{zi} \quad u_j \quad v_j \quad w_j \quad \theta_{yj} \quad \theta_{zj}\,]^T \tag{8}$$

where i and j (=i+1) are nodes. The shape functions are respectively defined as:

$$N_{t1} = 1 - s, N_{t2} = s, N_{t3} =$$
$$\frac{1}{1+\phi}\left[2s^3 - 3s^2 - \phi\, s + (1+\phi)\right],$$
$$N_{t4} = \frac{L}{1+\phi}\left[s^3 - \left(2 + \frac{\phi}{2}\right)s^2 + \left(1 + \frac{\phi}{2}\right)s\right],$$
$$N_{t5} = \frac{1}{1+\phi}\left[2s^3 - 3s^2 - \phi s\right],$$
$$N_{t6} = \frac{L}{1+\phi}\left[s^3 - \left(1 - \frac{\phi}{2}\right)s^2 - \left(\frac{\phi}{2}\right)s\right],$$
$$N_{\theta1} = -N_{\theta3} = \frac{6}{(1+\phi)L}\left(s^2 - s\right)$$
$$N_{\theta2} = \frac{1}{1+\phi}\left[3s^2 - (4+\phi)s + (1+\phi)\right],$$
$$N_{\theta4} = \frac{1}{1+\phi}\left[3s^2 - (2-\phi)s\right],$$
$$\text{where } \phi = \frac{12EI}{k_s AGL^2},\ \text{s} = \frac{\text{x}}{\text{L}}$$

By substituting the expressions for u, v, w, θ_x, θ_y in terms of shape functions into the expressions for T, V, and W and applying the Hamilton principle $\delta \int_{t_1}^{t_2} (T - V + W) = 0$, (where δ is the variational operator), the following finite element matrix form of equations are obtained:

$$[M_b]\{\ddot{q}\} - \Omega[G_b]\{\dot{q}\} + \left([K_b] + [K_{bP}] - \Omega^2[M_{bC}]\right)\{q\} = \{F_b\} \tag{9}$$

Here,

$$[M_b] = \int_0^L \rho A N_a^T N_a ds + \int_0^L \rho A N_t^T N_t ds + \int_0^L \rho I_d N_\theta^T N_\theta ds \tag{10}$$

$$[K_b] = \int_0^L EA N_a'^T N_a' ds + \int_0^L EI N_\theta'^T N_\theta' ds + \int_0^L kGA\left\{N_t'^T N_t' + N_\theta^T N_\theta + 2N_t'^T \begin{bmatrix} 0 & -1 \\ 1 & 0 \end{bmatrix} N_\theta\right\} ds \tag{11}$$

$$[G_b] = \int_0^L \rho J N_\theta^T \begin{bmatrix} 0 & 1 \\ -1 & 0 \end{bmatrix} N_\theta ds \tag{12}$$

Here $[M_b]$, $[K_b]$ and $[G_b]$ are the element mass, stiffness and gyroscopic matrices, respectively. Furthermore, the stiffness matrix with axial effect $[K_{bP}]$ along with centrifugal effects $[M_{bC}]$ are also included in the calculation. The concentrated and distributed forces were included in the force vector $\{F_b\}$. The details of the elemental mass, stiffness and gyroscopic matrices are separately given in the "Appendix A".

The spindle-tool system is supported on two radial rolling element bearings. The stiffness of bearings is considered in terms of axial preload as:

$$K_{xx} = K_{yy} = 1.77236 \times 10^7 \times \left(N_b^2.D_b\right)^{1/3} \frac{\cos^2\theta}{\sin^{1/3}\theta} F_a^{1/3} \text{ N/m} \tag{13}$$

where N_b is the number of balls, D_b is diameters of the ball, F_a is axial preload and θ is contact angle. The FRF consisting of real and imaginary parts which can be expressed directly as follows:

$$[H(i\omega_c)] = [\mathrm{Re}(\omega_c)] + i[\mathrm{Im}(\omega_c)] = [-[M_b]\omega_c^2 + i\omega_c[-\Omega[G_b]] + ([K_b + [K_b]_P - \Omega^2[M_b]_C)]^{-1} \tag{14}$$

Here, *Im and Re* are correspondingly the imaginary and real parts of the frequency responses.

2.2 *Interface elasticity model*

Most important parts are interfaces between the components and these interfaces are linear tapered regions and are modeled with variable nonlinear contact forces. In the present task linear spring element modeling is adopted and the spring stiffnesses are considered in both the lateral directions. The line contact region between the tool and holder is modeled with two springs while, that of the holder and spindle junction is modeled using three spring elements. The finite element model of the entire system discretized into eight segments and is shown in figure 2.

The interface springs join the nodes of respective coupling elements namely tool-holder and holder-spindle combinations, so as to get the revised assembled stiffness matrix.

3. Identification study

The frequency-domain responses can be characterized by statistical parameters such as peak-to-peak amplitude, mean value, rms value etc. The discrete frequency response signal over a frequency range is treated as a data set $N = \{x_1, x_2, \ldots, x_n\}$ of size n. Then the parameters such as mean, root mean-square value, variance, skewness, kurtosis etc. represents the signal indirectly. The parameters considered in present case are defined as:

$$\text{(i) Mean square value} \quad X_1 = \frac{1}{N}\sum_{i=0}^{N-1} x_i^2 \tag{15}$$

$$\text{(ii) Variance} \quad X_2 = \frac{1}{N-1}\sum_{i=0}^{N-1} (x_i - \mu)^2 \tag{16}$$

$$\text{(iii) Skewness} \quad X_3 = \frac{\sum_{i=0}^{N-1} (x_i - \mu)^3}{(N-1)\sigma^3} \tag{17}$$

$$\text{(iv) Kurtosis} \quad X_4 = \frac{\sum_{i=0}^{N-1} (x_i - \mu)^4}{(N-1)\sigma^4} \tag{18}$$

Where $\mu = \frac{1}{N}\sum_{i=0}^{N-1} x_i$ is mean or average value of the data. The parameters for both experimental and numerical frequency response signals can then be compared and the following error function to be minimized is defined:

$$(E(k_1, k_2, ..k_5, \eta_1, \eta_2, ...\eta_5)) = w_1\left(X_{\exp,1} - X_1\right)^2 + w_2\left(X_{\exp,2} - X_2\right)^2 + w_3\left(X_{\exp,3} - X_3\right)^2 + w_4\left(X_{\exp,4} - X_4\right)^2$$

where the E is the total error between the experimental and theoretical sampling data, w_i are the weights indicating the equal importance of each statistical parameter and suffix *exp* indicates the experimental response data. The upper and lower boundaries of the stiffness parameters k_1, k_2,… are selected as 1×10^6 to 1×10^8 N/m and that of structural damping factors η_1, η_2,.. are 0 and 1. For minimization of above objective function, genetic algorithms with elitism is employed and the results are validated with simulated annealing scheme.

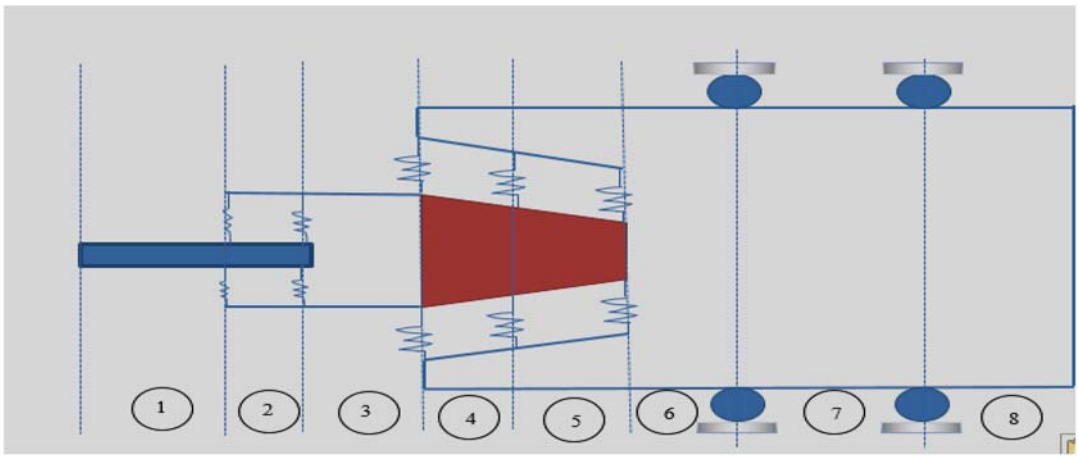

(a) Beam Model

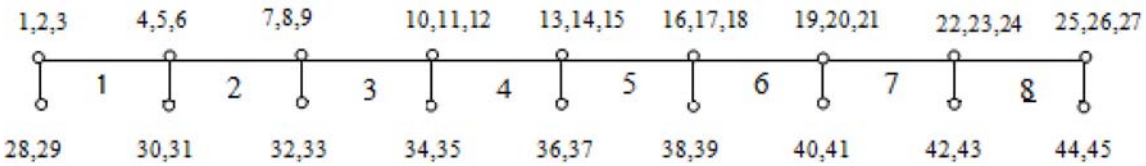

(b) Node numbering with elemental degrees of freedom

Figure 2. Beam model for the integrated spindle-tool unit with contact springs.

3.1 *Genetic algorithms*

Genetic algorithm (GA) is a branch of evolutionary computing, which is a rapidly growing area of artificial intelligence for optimizing design parameters for the spindle-tool unit. Genetic algorithms are based on the mechanics of natural selection and natural genetics and follow the Darwinian principle of survival of the fittest. The main organisms have to survive in the given environmental conditions which decides the basic principle of the evolutionary process. There are several methods of selecting operators like reproduction, representation, selection, etc. In the method of the selection process, several strategies such as roulette wheel selection and tournament are famous schemes. Once the population has been generated, the following steps are followed such as the coding, defining the fitness function for the maximization of minimization problems, reproduction followed by the crossover and mutation to generate the new set of population. Further, these new populations are further tested for the determination and this completes one generation and this process continues till the required criteria have been attained. The detailed process of the GA is shown in figure 3.

3.2 *Simulated annealing (SA)*

In view of the global optimization problem, simulated annealing is one of the best meta-heuristic optimization approaches in dealing with the global optimum solution in a large space with a higher rate of accuracy. This method can be conveniently applied to the discrete as well as with the large space with a prime goal of achieving a better accurate solution instead of the best possible solution. The basic idea comes from the metallurgy process, where the metal is heated at the prerequisite temperature and properly controlled heating to modify the grain structure of the metal to get the required properties and possibly by reducing the defects in the metal. To execute the optimization algorithm, the following steps are applied and as follows:

SA parameters: To determine the quality of the SA placement the correct assumption of the operational parameters and its functions need to be identified. For most of the optimization algorithms, calculation of gradient descent is essentially required whereas for the SA it is not required. SA is very easy to program and coding can be finished in a few lines. Further, this can be applied to different types of engineering problems with various constraints. SA can be applied to any type of problem without

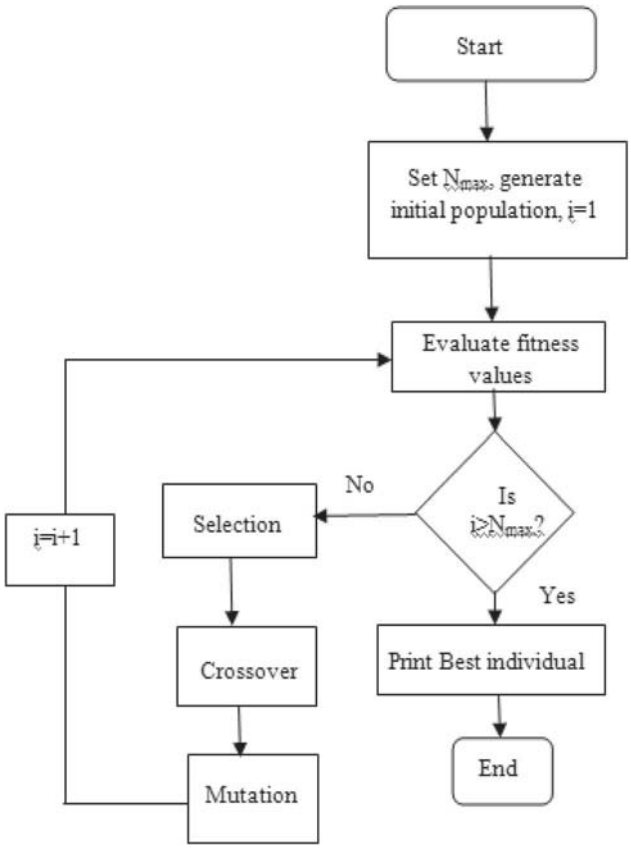

Figure 3. Flowchart for genetic algorithms.

knowing the initial conditions and can be able to determine the global minimum efficiently for a large space. In general, the algorithm needs four basic components such as (i) Configurations, (ii) Move set, (iii) Cost Function and (iv) Cooling Schedule.

(i) **Configurations:** It mainly represents the probable possible solution for the problem in different spaces. Mathematically, the search function reduces the maximum number of matrices from the given set of configurations with several parameters ($x = x_1, x_2 \ldots, x_n$)

(ii) **Move set:** Basically it is the perturbation scheme to improve the current solution with the easiness of getting various sets.

(iii) **Cost function:** This function is mainly employed to find the variation between the current and the previous solution sets. Based on these errors, then the given set can be accepted or rejected by using the Metropolis condition. A random number has to be selected between 0 to 1 if the given configuration is worse than the previous one.

(iv) **Cooling Schedule:** In order to obtain a good solution, the selection of placement algorithms with a high value of initial temperature T is required. According to the close degree of approximation, the annealing temperature has to be specified by the programmer. Generally, the selection of initial or starting temperature must be high, because it can enhance the search space for the given state of the problem. Further, the final or cooling temperature should be closed to zero but not exactly zero. In between these approximations, the size of the problem is directly related to the considerable number of iterations for each possible set. Furthermore, the iterations at each step are defined by the temperature. The probability of finding the local optimum can be obtained in a wide range possibly by the lower temperatures.

4. Results and discussions

4.1 *Finite element methodology*

The undesired vibration levels that occurred between the cutting tool and workpiece during the machining process, is due to the excess input energy levels when compared with the dissipation of the energy. To model the integrated spindle tool system, the geometrical dimensions and the material properties are considered from the user manuals of the MTAB MAXMILL CNC vertical end mill. The model parameters for the finite element modeling of the integrated unit are given in table 1.

The cutting tool is firmly coupled to the tool holder and its length can be adjusted inside the holder to get the required overhang length. Further, this connection is placed in the taper portion of the spindle and it relies on the angular contact ball bearings. A computer program is developed in the MATLAB software to analyze the integrated spindle dynamics at the tool-tip. The comparative analysis has been carried out on the entire spindle-tool system to evaluate the frequency response at the tool-tip. In the initial case, the model is assumed to be rigidly coupled at the interfaces whereas in the second case the coupling between the interfaces of the spindle-holder-tool is modeled with the distributed springs over the tapered length.The entire structure is divided into eight elements with only translational degrees of freedom at each node by considering the radial stiffness of springs as 1.5×10^5 N/m. The rotational degree of freedom at each node was eliminated with the Guyan reduction method. The comparative plots of frequency response for the two cases are shown in figure 4. It is evident that for the distributed spring model coupling the fundamental mode of frequency is around 1981 Hz whereas for the rigid coupling interface the frequency is around 2059 Hz.

Convergence tests are carried out on the present finite element model to minimize discretization errors by increasing the number of degrees of freedom (DOF). It is

Table 1. Integrated spindle tool parameters for the finite element model.

Parameters	Elements of the spindle tool unit							
	#1	#2	#3	#4	#5	#6	#7	#8
Length (mm)	30	30	85	51	60	45	45	47
Outer diameter (mm)	12	12	40	75	75	75	75	75
Inner diameter (mm)	0	0	0	40	0	0	0	0
E (Pa)	2.8×10^{11}	2.1×10^{11}	2.1×10^{11}	2.1×10^{11}	2.1×10^{11}	2.1×10^{11}	2.1×10^{11}	2.1×10^{11}
Density (kg/m^3)	7972	7850	7850	7850	7850	7850	7850	7850

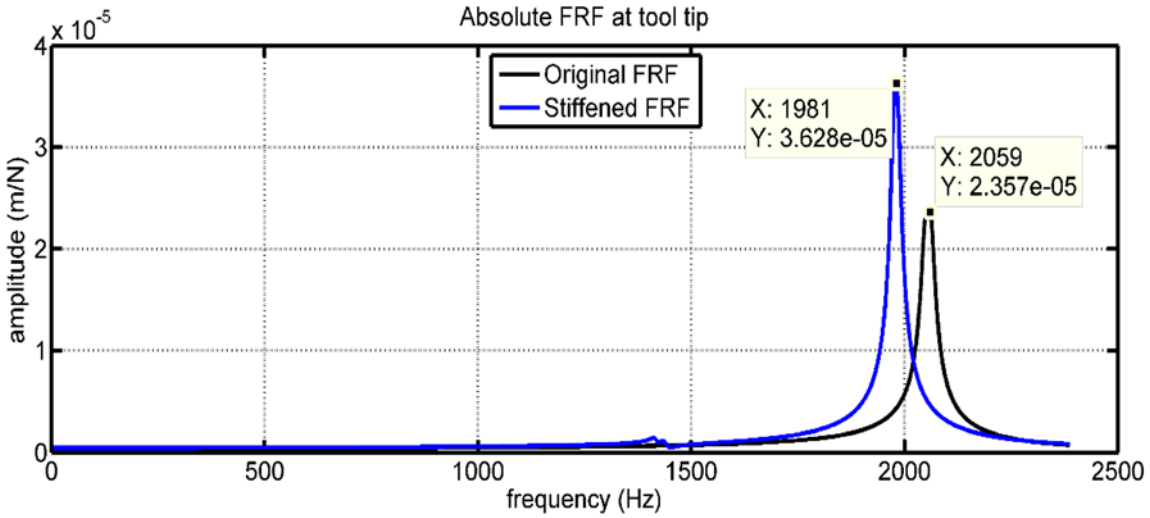

Figure 4. Tooltip FRF with rigid and contact stiffness.

Table 2. Convergence results of natural frequencies of the spindle tool unit.

Sl. No.	Natural frequency (Hz)
3 elements	2055.8
5 elements	2057.68
7 elements	2058.15
8 elements	2059.45
12 elements	2059.45
16 elements	2059.45

observed from table 2 that after eight elements it maintains the same frequency value.

The eight-element model considered has 45 degrees of freedom and the rotational degrees of freedom were eliminated by using the Guyan reduction scheme.

4.2 *Experimental analysis*

In the present paper, modal analysis is conducted on the CNC end mill with the maker from MTAB-MAXMILL with the Fanuc system. This machine tool has a single spindle with three axes and a single-phase motor with the possibility of operating at different rotational speeds. The following equipment is utilized to obtain the natural frequencies of the spindle-tool system. (i) Oscilloscope with four operating channels to record the time histories of vibration levels with model no DPO-43034. (ii) A vibration shaker to excite the system at the tool-tip with the type V-6-27050. (iii) A signal generator to produce various forms of sine and cosine waveforms at different frequency levels. (iv) A charge amplifier with a frequency range from 0.3 Hz to 20 KHz. (v) An accelerometer to measure the excitations of the tool-tip with the model no: PG109M0 and it has min to a max frequency of 1 Hz to 10 kHz. (vi) A power amplifier to boost up the amplitude of the input signal. The arrangement of all these equipment is shown in figure 5.

Modal testing is conducted on the CNC spindle tool system by varying the frequency levels with a signal generator at the constant amplitudes by operating with the power amplifier. This signal generator excites the vibration shaker, pointed at the tip of the cutting tool at different ranges of frequency produces the displacements at the tip of

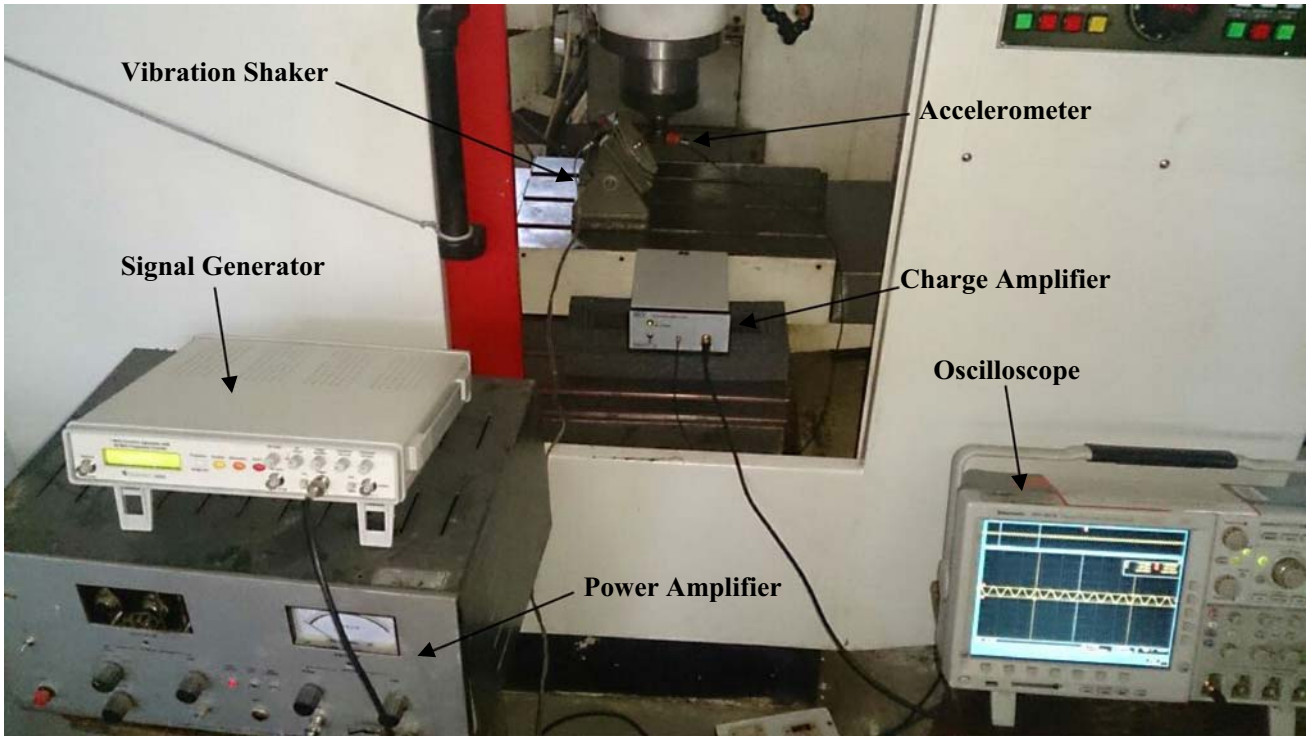

Figure 5. Modal testing experimental set-up.

the cutting tool. These vibration signals are measured by the accelerometer attached at the shank portion of the cutting tool and further, these signals are recorded in the four-channel digital oscilloscope. The amplitude of these time domains at different frequency levels are noted and further these amplitude data were plotted against the corresponding frequency levels as shown in figure 6.

It is observed from the plot that there are two sweeping range frequencies of 1995 Hz to 2585 Hz respectively. This first mode had a better agreement with the frequency obtained from the finite element approach.

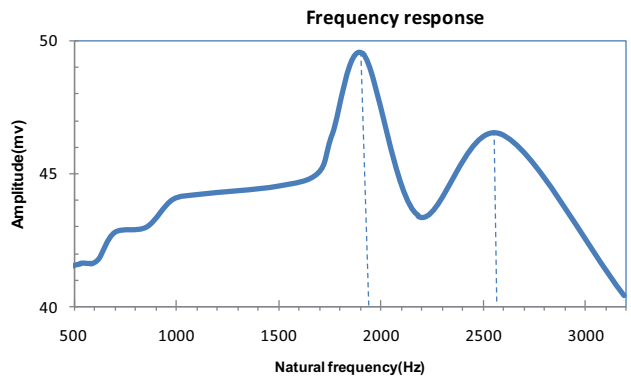

Figure 6. Experimental frequency response plot from the modal testing.

Further, the contact stiffness values of the springs are varied to observe the pattern of frequency response at the tool-tip, and the corresponding variation is shown in figure 7. It is observed that, when the contact stiffness of the distributed springs increases, there is an increment in the fundamental frequency and a reduction in the corresponding vibration amplitude levels as seen in figure 7(a). Similarly, the real and imaginary parts of the frequency response of the tool-tip for the three values of contact stiffness are shown in figure 7(b).

Furthermore, instead of considering the individual stiffness of the contact springs, the contact stiffness is varied along the tapered length of the spindle-holder interface at different connecting nodes. To employ the stiffness, an elastic layer of constant coupling stiffness coefficient K(x) is introduced in the finite element modeling as a function of normal pressure at the interfaces. During the machining process, it is to be assumed that there should be no slipping between the interfaces for a constant value of the coupling stiffness coefficient. The elastic interface stiffness is included in the MATLAB program as a complex-valued coefficient $K(x) = k(1 + i\eta)$, where the k is the interface contact stiffness and η is the structural damping factor.

The selection of structural damping at interfaces provides better stability during the machining process. In the present case, the different structural damping factors are considered at the interfaces and the corresponding frequency responses arrive at the tooltip as shown in figure 8.

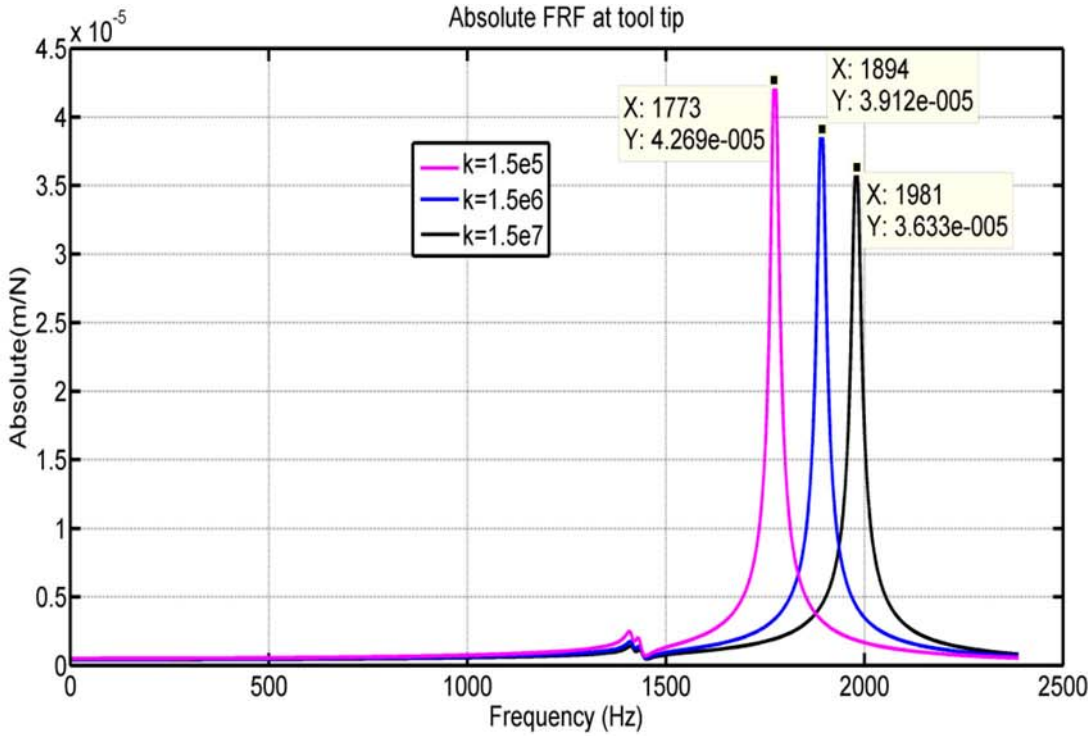

(**a**) Absolute frequency response at the tooltip

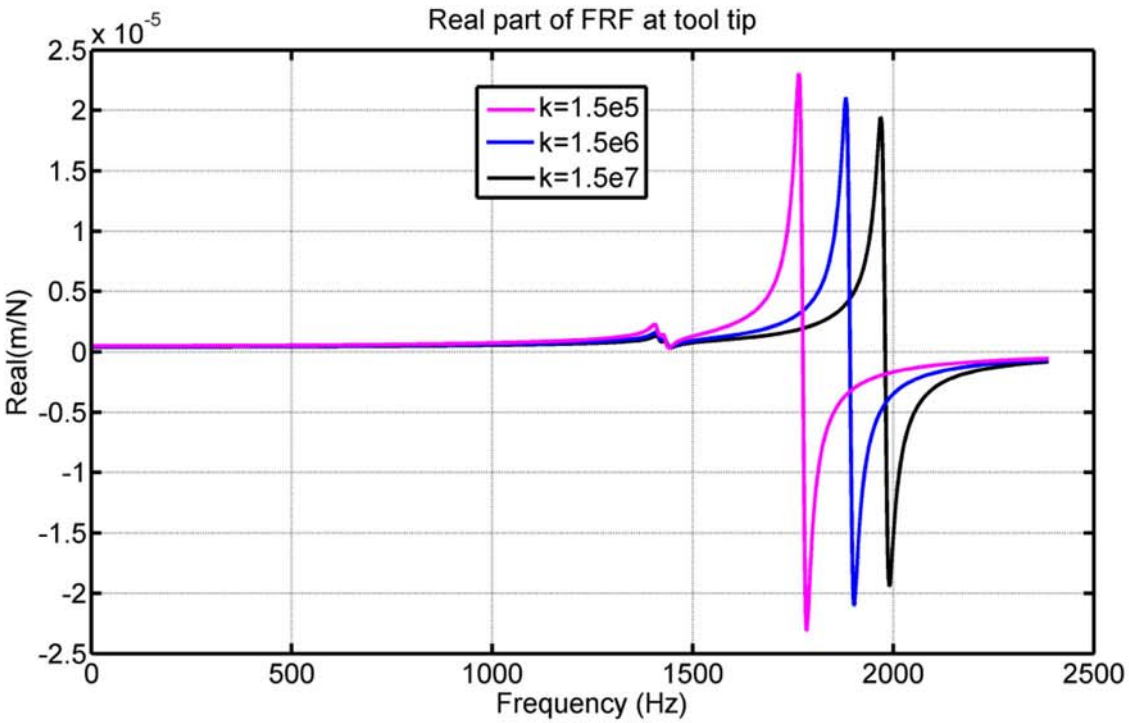

(**b**) Real part frequency response at the tooltip

Figure 7. Frequency responses with the variation in the contact stiffness.

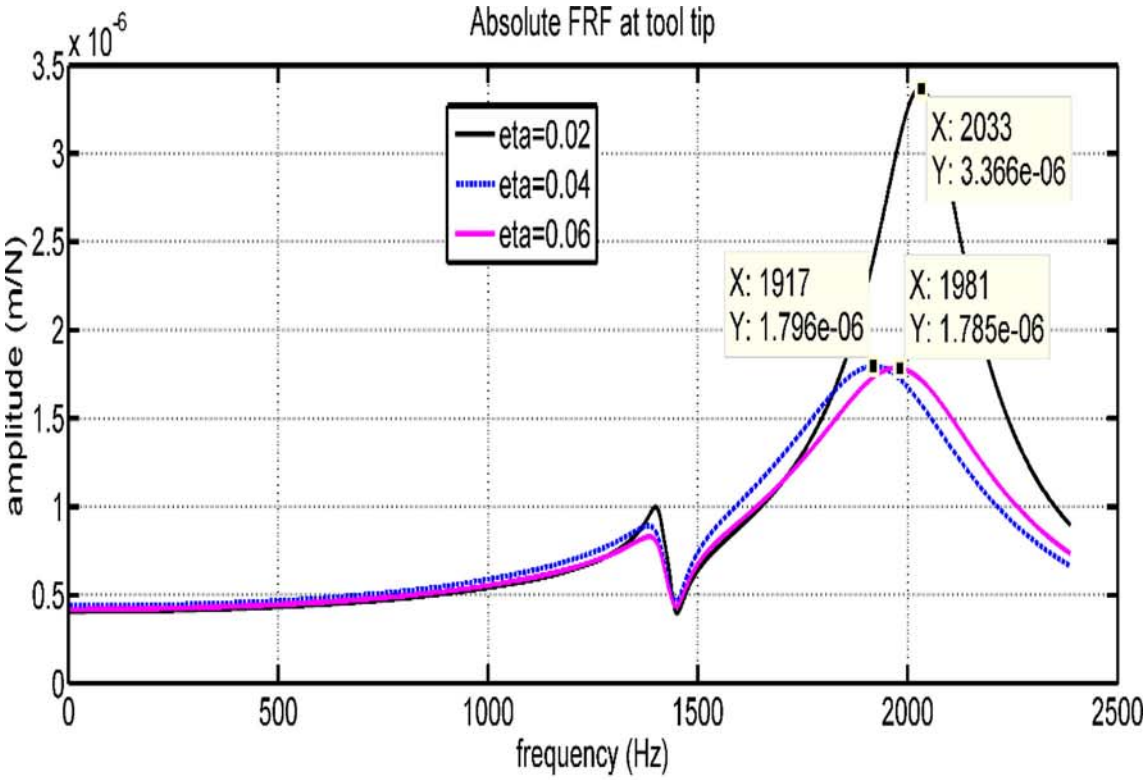

(a) Absolute FRF

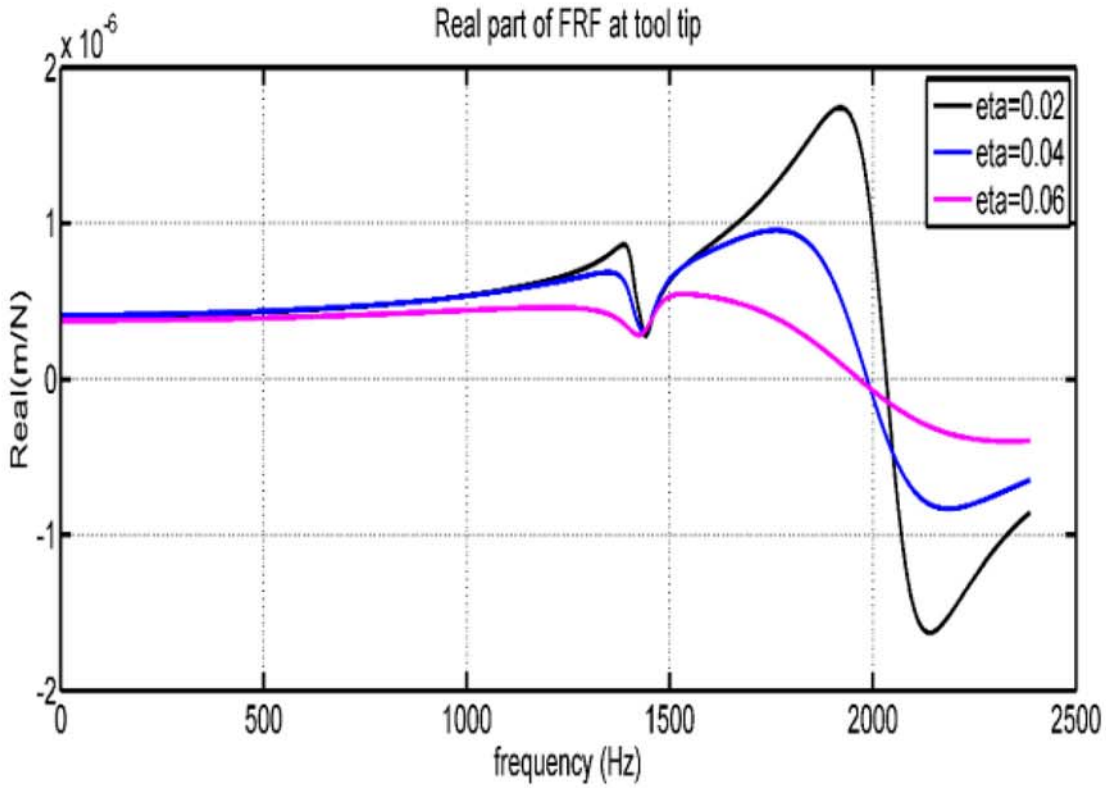

(b) Real part of FRF

Figure 8. Tooltip FRF plots for different structural damping factors.

Table 3. Statistical design parameters for the frequency domain.

Sl. No.	Contact stiffness	Structural damping factor	Sum of squares (X_1)	Variance (X_2)	Skewness (X_3)	Kurtosis (X_4)
1	1.5e5	0.02	0.81	0.24	0.55	0.69
2	1.5e5	0.04	0.83	0.38	0.35	0.54
3	1.5e5	0.06	0.82	0.23	0.54	0.60
4	1.5 e6	0.02	0.85	1.00	1.00	1.00
5	1.5 e6	0.04	0.89	0.30	0.25	0.56
6	1.5 e6	0.06	0.88	0.33	0.32	0.52
7	1.5 e7	0.02	1.00	0.68	0.56	0.49
8	1.5 e7	0.04	0.95	0.70	0.32	0.37
9	1.5 e7	0.06	0.93	0.79	0.27	0.35

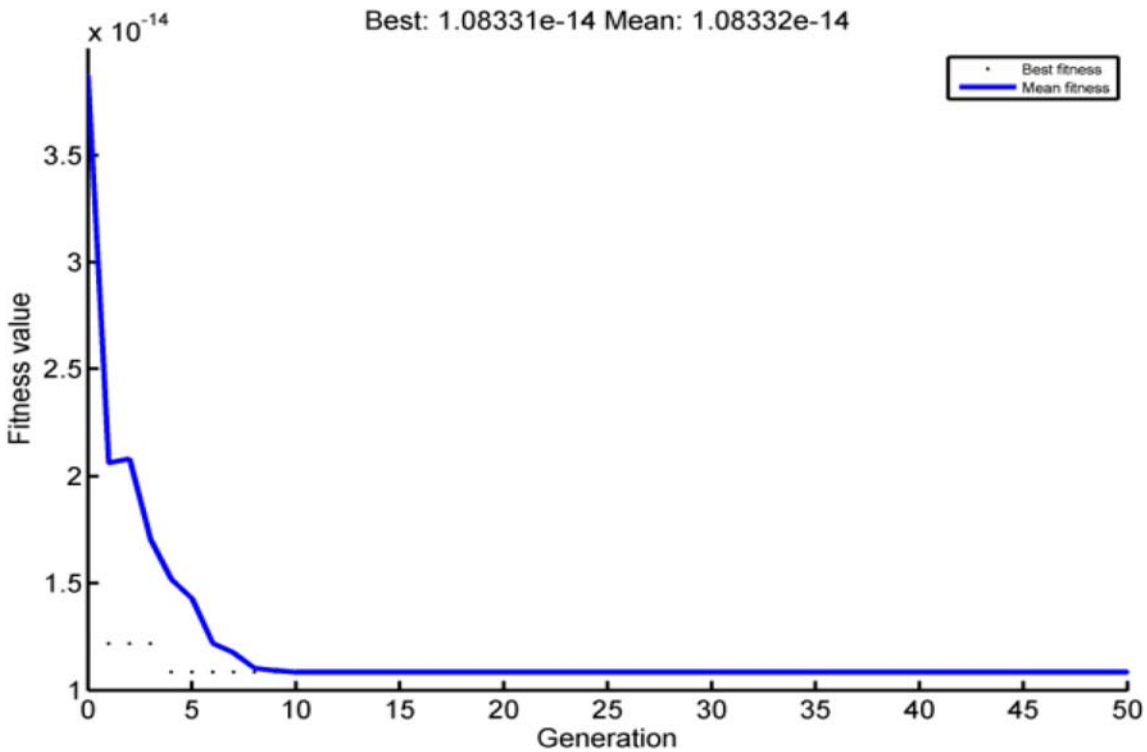

Figure 9. Convergence trend using the Genetic algorithms.

It is observed from the plots that the damping factor of 0.06, gives the fundamental frequency of 1981 Hz and it is in a closer degree of agreement with the experimental modal testing. The corresponding real and imaginary parts of the absolute frequency responses are shown in figures 8(a) and 8(b). The structural damping factor values are varied to match the fundamental frequency of the system. It is observed that a combination of radial stiffness 1.5×10^7 N/m and structural damping factor of 0.06 is close with the experimental value.

In the present analysis, the tool-tip frequency responses arrived for different combinations of contact stiffness and structural damping factors. A sampling rate of 10 kHz is used to obtain the frequency response. The statistical design parameters are evaluated for all these sampling units as given in table 3.

The primary target for the optimization process is to minimize the error between the experimental sampling data with the theoretical data.

The GA process is simulated by using the MATLAB toolbox with the following parameters: (i) Number of generations = 90, (ii) Population size = 20, (iii) Cross-over probability = 0.9 and (iv) Mutation probability = 0.001. The convergence pattern as observed using the GA technique is shown in figure 9.

Table 4. Optimal statistical data of SA and GA.

Sl. no.	Statistical parameters	Simulated annealing	Genetic algorithm	Theoretical static design factors
1	Sum of squares (X_1)	0.932	0.927	0.93
2	Variance (X_2)	0.788	0.785	0.79
3	Skewness (X_3)	0.278	0.269	0.27
4	Kurtosis (X_4)	0.349	0.345	0.35

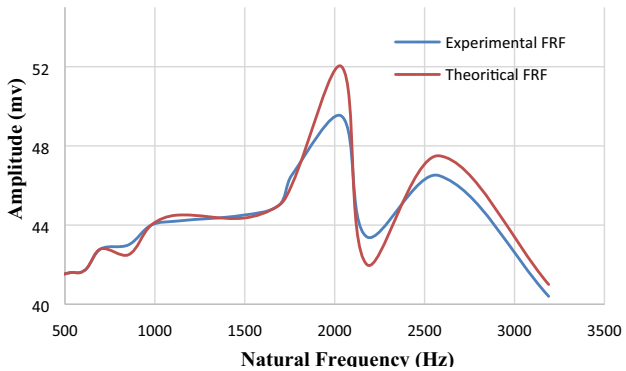

Figure 10. Tool-tip FRF with normalized amplitudes.

Results of GA are validated with simulated annealing method with the following parameters: initial temperature = 100 with exponential temperature function and fast annealing cooling rate. The best optimal values obtained from these two meta-heuristic algorithms are depicted in table 4. It is observed that the optimal values obtained from these two algorithms are close to each other. Using the values of contact stiffness 1.566×10^7 N/m and a structural damping factor 0.0612, the optimal values are obtained for these simulation algorithms.

The frequency response curves with the normalized amplitudes are plotted for both the experimental and the optimized parameter finite element model as shown in figure 10. It is observed that the fundamental frequency mode for the theoretical analysis is 1998 Hz, and this value is close to the experimental modal frequency of 1991 Hz.

5. Conclusions

Interface stiffness parameter identification approach was presented in this work using a tool-tip frequency response error minimization. The spindle and holder portions were modeled as solid beam elements and their interfaces are modeled with the contact springs. The following points are summarized:

- Convergence tests were carried out to verify the adequacy of the tool interface model.
- In the tool-holder interface modeling, the distributed parameter joint interfaces with a change in the structural damping factor as well as the contact stiffness were effectively considered.
- An experimental study was conducted to obtain the true frequency response data.
- The equivalent statistical parameters were considered for representing the frequency responses at different combinations of stiffness and structural damping factors.
- Genetic algorithm scheme was employed to minimize the total error function and the results were found to be in good agreement with those obtained from simulated annealing optimization.
- Futher, a frequency response plot with the optimized values is compared with experimental frequency and it is evident that the responses are in closer agreement.

The modular programs developed in the present work facilitate in providing the accuracy for evaluating the frequency responses at the tool tip with flexible stiffness and damping parameters.

List of symbols

K_{xx}= K_{yy}	Static radial stiffness in x and y direction at the bearing nodes
D_b	Ball diameter
F_a	Bearing preload
θ	Contact angle of static angular-contact ball bearing
N_b	Number of balls
ω_c	Chatter frequency
A	Cross-sectional area of beam
E, G, J	Young's, Shear modulus and Polar moment of inertia of the beam
K_s	Timoshenko's shear coefficient and it is taken as 0.9
ψ	Transverse shear effect
ρ	Density of the beam material
L	Length of the beam portion

Appendix A

The elemental mass, stiffness and gyroscopic matrices are given below

$$[M] = [M]_T + [M]_R$$

where *[M]$_T$* and *[M]$_R$* are the translational and rotational mass matrices.

$$[M]_T = \frac{\rho AL}{420(1+\psi)^2}$$

$$\begin{bmatrix}
m_{a1} & & & & & & & & & \\
0 & m_1 & & & & & & & & \\
0 & 0 & m_1 & & & S & & & & \\
0 & 0 & -m_2 & m_5 & & & Y & & & \\
0 & m_2 & 0 & 0 & m_5 & & & M & & \\
m_{a2} & 0 & 0 & 0 & 0 & m_{a1} & & & & \\
0 & m_3 & 0 & 0 & -m_4 & 0 & m_1 & & & \\
0 & 0 & m_3 & m_4 & 0 & 0 & 0 & m_1 & & \\
0 & 0 & -m_4 & m_6 & 0 & 0 & 0 & m_2 & m_5 & \\
0 & m_4 & 0 & 0 & m_6 & 0 & -m_2 & 0 & 0 & m_5
\end{bmatrix}$$

$$[M]_R = \frac{\rho I}{30(1+\psi)^2 L}$$

$$\begin{bmatrix}
0 & & & & & & & & & \\
0 & 36 & & & & & & & & \\
0 & 0 & 36 & & & S & & & & \\
0 & 0 & -m_7 & m_8 & & & Y & & & \\
0 & m_7 & 0 & 0 & m_8 & & & M & & \\
0 & 0 & 0 & 0 & 0 & 0 & & & & \\
0 & -36 & 0 & 0 & -m_7 & 0 & 36 & & & \\
0 & 0 & -36 & m_7 & 0 & 0 & 0 & 36 & & \\
0 & 0 & -m_7 & m_9 & 0 & 0 & 0 & m_7 & m_8 & \\
0 & m_7 & 0 & 0 & m_9 & 0 & -m_7 & 0 & 0 & m_8
\end{bmatrix}$$

The mass matrix *[M$_c$]* is used to compute the centrifugal force is given by

$$[M]_C = \frac{\rho AL}{420(1+\psi)^2}$$

$$\begin{bmatrix}
0 & & & & & & & & & \\
0 & m_1 & & & & & & & & \\
0 & 0 & m_1 & & & S & & & & \\
0 & 0 & -m_2 & m_5 & & & Y & & & \\
0 & m_2 & 0 & 0 & m_5 & & & M & & \\
0 & 0 & 0 & 0 & 0 & 0 & & & & \\
0 & m_3 & 0 & 0 & -m_4 & 0 & m_1 & & & \\
0 & 0 & m_3 & m_4 & 0 & 0 & 0 & m_1 & & \\
0 & 0 & -m_4 & m_6 & 0 & 0 & 0 & m_2 & m_5 & \\
0 & m_4 & 0 & 0 & m_6 & 0 & -m_2 & 0 & 0 & m_5
\end{bmatrix}$$

$m_1 = 156 + 294\psi + 140\psi^2$; $m_2 = (22 + 38.5\psi + 17.5\psi^2)L$; $m_3 = 54 + 126\psi + 70\psi^2$; $m_4 = -(13 + 31.5\psi + 17.5\psi^2)L$; $m_5 = (4 + 7\psi + 3.5\psi^2)L^2$; $m_6 = -(3 + 7\psi + 3.5\psi^2)\ L^2$;$m_7 = (3 - 15\psi)L$; $m_8 = (4 + 5\psi + 10\psi^2)L^2$; $m_9 = (-1 - 5\psi + 5\psi^2)L^2$;

$$m_{a1} = 140(1+\psi)^2; m_{a2} = 70(1+\psi)^2; \psi = \frac{12EI}{K_s AGL^2}$$

The gyroscopic matrix *[G]* is:

$$[G] = \frac{\rho J}{30(1+\psi)^2 L}$$

$$\begin{bmatrix}
0 & & & & & & & & & \\
0 & 0 & & & SKEW & & & & & \\
0 & 36 & 0 & & & S & & & & \\
0 & -m_7 & 0 & 0 & & & Y & & & \\
0 & 0 & -m_7 & m_8 & 0 & & & M & & \\
0 & 0 & 0 & 0 & 0 & 0 & & & & \\
0 & 0 & 36 & -m_7 & 0 & 0 & 0 & & & \\
0 & -36 & 0 & 0 & -m_7 & 0 & 36 & 0 & & \\
0 & -m_7 & 0 & 0 & -m_9 & 0 & m_7 & 0 & 0 & \\
0 & 0 & -m_7 & m_9 & 0 & 0 & 0 & m_7 & m_8 & 0
\end{bmatrix}$$

The stiffness matrix *[K]* is given by

$$[K]_C = \frac{EI}{(1+\psi)L^3}$$

$$\begin{bmatrix}
k_1 & & & & & & & & & \\
0 & 12 & & & & & & & & \\
0 & 0 & 12 & & & S & & & & \\
0 & 0 & -6L & k_2 & & & Y & & & \\
0 & 6L & 0 & 0 & k_2 & & & M & & \\
-k_1 & 0 & 0 & 0 & 0 & k_1 & & & & \\
0 & -12 & 0 & 0 & -6L & 0 & 12 & & & \\
0 & 0 & -12 & 6L & 0 & 0 & 0 & 12 & & \\
0 & 0 & -6L & k_3 & 0 & 0 & 0 & 6L & k_2 & \\
0 & 6L & 0 & 0 & k_3 & 0 & -6L & 0 & 0 & k_2
\end{bmatrix}$$

$$k_1 = A(1+\psi)\frac{L^2}{I}; k_2 = (4+\psi)L^2; k_3 = (2-\psi)L^2$$

$$[K]_P = \frac{P_a}{30(1+\psi)L}$$

$$\begin{bmatrix}
0 & & & & & & & & & \\
0 & k_4 & & & & & & & & \\
0 & 0 & k_4 & & & S & & & & \\
0 & 0 & -3L & k_5 & & & Y & & & \\
0 & 3L & 0 & 0 & k_5 & & & M & & \\
0 & 0 & 0 & 0 & 0 & 0 & & & & \\
0 & -k_4 & 0 & 0 & -3L & 0 & k_4 & & & \\
0 & 0 & -k_4 & 3L & 0 & 0 & 0 & k_4 & & \\
0 & 0 & -3L & k_6 & 0 & 0 & 0 & 3L & k_5 & \\
0 & 3L & 0 & 0 & k_6 & 0 & -3L & 0 & 0 & k_5
\end{bmatrix}$$

$k_4 = 36 + 60\psi + 30\psi^2; k_5 = (4 + 5\psi + 2.5\psi^2)L^2;$

$k_6 = -(1 + 5\psi + 2.5\psi^2)L^2;$

References

[1] Schmitz T 2020 Modal interactions for spindle, holders and tools. *Proc. Manufacturing.* 48: 457–465.

[2] Xu K, Wang B, Zhao Z, Zhao F, Kong X and Wen B 2020 The influence of rolling bearing parameters on the nonlinear dynamic response and cutting stability of high-speed spindle systems. *Mechanical Systems and Signal Processing.* 136: 106448. https://doi.org/10.1016/j.ymssp.2019.106448

[3] Namazi M, Altintas Y, Abe T and Rajapakse N 2007 Modeling and identification of tool holder–spindle interface dynamics. *International Journal of Machine Tools & Manufacture.* 47: 1333–1341

[4] Bossmanns B and Tu J F 2002 Conceptual design of machine tool interfaces for high-speed machining. *Journal of Manufacturing Processes.* 4(1): 16–27

[5] Agapiou J S 2005 A methodology to measure joint stiffness parameters for tool holder-spindle interfaces. *Journal of Manufacturing Processes.* 24(1): 13–20

[6] Xiao W, Mao K, Zhu M, Li B, Lei S and Pan X 2014 Modelling the spindle–holder taper joint in machine tools: A tapered zero-thickness finite element method. *Journal of Sound and Vibration.* 333: 5836–5850

[7] Zahedi A and Movahhedy M R 2012 Thermo-mechanical modeling of high speed spindles. *ScientiaIranica B.* 19(2): 282–293

[8] Zivkovic A, Zeljkovic M, Tabakovic S and Milojevic Z 2015 Mathematical modeling and experimental testing of high-speed spindle behavior. *Int. J. Adv. Manuf. Technol.* 77: 1071–1086

[9] Cao Y and Altintas Y 2004 A general method for the modelling of spindle-bearing systems. *J. Mech. Des., Transactions of the A S M E.* 126: 1089–1104

[10] Altintas Y and Cao Y 2005 Virtual design and optimization of machine tool spindles. *Annals of CIRP.* 54(1): 379–382

[11] Suzuki N, Kurata Y, Kato T, Hino R and Shamoto E 2012 Identification of transfer function by inverse analysis of self-excited chatter vibration in milling operations. *Precision Engineering.* 36: 568–575

[12] Gagnol V, PhuLe T and Ray P 2011 Modal identification of spindle-tool unit in high-speed machining. *Mechanical Systems and Signal Processing.* 25: 2388–2398

[13] Cao H, Li B and He Z 2013 Finite Element Model Updating of Machine-Tool Spindle Systems. *Journal of Vibration and Acoustics.* 135: 0245031–0245034

[14] Chi M, Xuesong M, Jun Y, Liang Z and Hu S 2015 Thermal characteristics analysis and experimental studyon the high-speed spindle system. *Int. J. Adv. Manuf. Technol.* 79: 469–489

[15] Mehrpouya M, Graham E and Park S S 2013 Frequency response function based joint dynamics modelling and identification. *Mechanical Systems and Signal Processing.* 39: 265–279

[16] Ganguly V and Schmitz T L 2013 Spindle dynamics identification using particle swarm optimization. *J. Manufacturing Processes.* 15: 444–451

[17] Mohammad R M and Mosaddegh P 2006 Prediction of chatter in high speed milling including gyroscopic effects. *International Journal of Machine Tools & Manufacture.* 46: 996–1001

[18] Jiang S and Zheng S 2010 A modeling approach for analysis and improvement ofspindle-drawbar-bearing assembly dynamics. *International Journal of Machine Tools & Manufacture.* 50: 131–142

[19] Ahmed A D S and Atsushi M 2015 Investigation about the characterization of machine tool spindlestiffness for intelligent CNC ends milling. *Robotics and Computer-Integrated Manufacturing.* 34: 133–139

[20] Farid Muhammad, Koura M, Muhammad Lotfy Z and Ahmed Sayedshaaban A 2014 Simulation approach to study the behavior of a milling machine's structure during end milling operation. *Turkish Journal of Engineering & Environmental Sciences.* 38: 167–183

[21] Schmitz T L, Powell K, Won D, Duncan G S, Sawyer W G and Ziegert J C 2007 Shrink fit tool holder connection stiffness/damping modeling for frequency response prediction in milling. *International Journal of Machine Tools & Manufacture.* 47: 1368–1380

[22] Xu C, Zhang J, Feng P, Yu D and Wu Z 2014 Characteristics of stiffness and contact stress distribution of a spindle–holder taper joint under clamping and centrifugal forces. *International Journal of Machine Tools & Manufacture.* 83: 21–28

[23] Gao X, Wang M, Zhang Y and Zan T 2015 A modeling approach for contact stiffness of spindle–tool holder based on fractal theory. *Engineering Manufacturing Part-B Proc. IMech E..* https://doi.org/10.1177/0954405415579009.

[24] Matthias W, Ozsahin O, Altintas Y and Denkena B 2016 Receptance coupling based algorithm for the identification of contact parameters at holder–tool interface. *CIRP Journal of Manufacturing Science and Technology.* 13: 37–45

[25] Mehrpouya M, Sanati M and Park S S 2016 Identification of joint dynamics in 3D structures through the inversereceptance coupling method. *International Journal of Mechanical Sciences.* 105: 135–145

[26] Mohammadi Y, Azvar M and Budak E 2018 Suppressing vibration modes of spindle-holder-tool assembly through frequency response modification for enhanced chatter stability. *CIRP Annals.* 67: 397–400

[27] Liu J, Ma C, Wang S, Wang S and Yang B 2019 Contact stiffness of spindle-tool holder based on fractal theory and multi-scale contact mechanics model. *Mechancal Systems and Signal Processing.* 119: 363–379

[28] Chang Y, Ding J, He Z, Shehzad A, Ding Y, Lu H, Zhuang H, Chen P, Zhang Y, Zhang X and Chen Y 2020 Effect of joint interfacial contact stiffness on structural dynamics of ultra-precision machine tool. *Int. J. Mach. Tools and Manuf.* 158: 103609. https://doi.org/10.1016/j.ijmachtools.2020.103609

[29] Zain A M and Haron Hand Sharif S 2010 Simulated annealing to estimate the optimal cutting conditions for minimizing surface roughness in end milling Ti-6Al-4V. *Machining Science and Technology.* 14: 43–62

[30] Zain A M, Haron H and Sharif S 2011 Integration of simulated annealing and genetic algorithm to estimate optimal solutions for minimising surface roughness in end milling Ti-6AL-4V. *International Journal of Computer Integrated Manufacturing.* 24: 574–592

[31] Wang Z G, Wong Y S and Rahman M 2004 Optimisation of multi-pass milling using genetic algorithm and genetic simulated annealing. *Int. J. Adv. Manuf. Technol.* 24: 727–732

[32] Saffar R J and Razfar M R 2010 Simulation of end milling operation for Predicting cutting forces to minimize tool deflection by Genetic Algorithm. *Machining Science and Technology: An International Journal.* 14: 81–101

[33] Palanisamy P, Rajendran I and Shanmugasundaram S 2007 Optimization of machining parameters using genetic algorithm and experimental validation for end-milling operations. *Int. J. Adv. Manuf. Technol.* 32: 644–655

[34] Sathish S, Anandakrishnan V and Gupta M 2019 Optimization of tribological behavior of magnesium metal-metal composite using pattern search and simulated annealing techniques. *Materials Today: Proceedings.* https://doi.org/10.1016/j.matpr.2019.06.643

[35] Olvera D, Elías-Zúñiga A, Martínez-Alfaro H, López de Lacalle L N, Rodríguez C A and Campa F J 2014 Determination of the stability lobes in milling operations based on homotopy and simulated annealing techniques. *Mechatronics.* 24(3): 177–185

[36] Palacios J A, Olvera D, Urbikain G, Elías-Zúñiga A, Martínez-Romero O, López de Lacalle L N, Rodríguez C and Martínez-Alfaro H 2018 Combination of simulated annealing and pseudo spectral methods for the optimum removal rate in turning operations of nickel-based alloys. *Advances in Engineering Software.* 115: 391–397